Simulation for the Fault Current Limiting Operation of REBCO CORC Superconducting Cables With Different Core Materials

Linh N. Nguyen , Martin Naud, Jeremy Weiss , *Member, IEEE*, Sastry Pamidi , *Senior Member, IEEE*, Sven A. Dönges , Danko van der Laan , and Doan N. Nguyen

Abstract—With high power density and low loss, CORC superconducting cables composed of RE − Ba$_2$Cu$_3$O$_{7-\delta}$ (REBCO)-coated conductors are of great interest for power transmission applications. They can also effectively be designed to serve as fault current limiters, thanks to their sharp superconducting-to-normal transition. Coupled electromagnetic-thermal finite-element simulations implemented in COMSOL Multiphysics were developed and validated against the published results for the fault current limiting (FCL) performance of two CORC cables of REBCO-coasted conductors wound on either copper or stainless steel cores. For improved accuracy, temperature dependencies of electrical and thermal properties of all component materials were considered in the simulations. The simulations were performed in the cross sections of the cables for every individual layer of each REBCO tape to deliver comprehensive understanding of the evolution of the current distribution and temperature rise in those layers. The studies can suggest approaches to optimize cable design for FCL applications by assessing the role of individual components. In the article, possible computational errors, challenges, and improvements are also discussed.

Index Terms—CORC, fault current limiter, finite-element modeling (FEM), high-temperature superconducting, superconducting cable.

I. Introduction

THE second generation (2G) RE–Ba$_2$Cu$_3$O$_{7-\delta}$ (REBCO)-coated conductors have been available in long lengths with acceptable uniformity along the length, enabling successful

TABLE I
PROPERTIES OF REBCO CORC SUPERCONDUCTING CABLES

Parameters	Cu CORE	SS CORE
Number of layers	8	6
Number of tapes per layer	2	3
Former Diameter (mm)	2.4	3.2
Outer diameter (mm)	3.2	3.8
I_c at 76 K (A)	646	1124
HTS tape width (mm)	2	2
Kapton layer thickness (mm)	0.025	0.025

demonstrations of liquid nitrogen cooled HTS cables in the real electric power grid [1], [2], [3], [4]. High-temperature superconducting (HTS) power cables using 2G-coated conductors are particularly attractive to replace traditional metal conductors for power transmission and distribution applications that require power cables of higher power density, smaller size, and lighter weight. Additionally, the very fast and responsive nature of the transition from superconducting to a normal state when an HTS cable carries a current higher than its critical current can automatically suppress current surges caused by a fault on the power grid. This fault current limiting (FCL) feature of HTS cables possibly enables the development of much safer power transmission/distribution systems. Therefore, extensive research and development related to cable design have been done to test and improve the FCL capability of HTS cables [5], [6], [7], [8], [9], [10], [11]. Advanced Conductors Technologies in collaboration with the Center for Advanced Power Systems (CAPS) developed and tested FCL performance on 2 CORC cables, one has 8 layers of two 2G REBCO tapes wound on a copper core and the other has 6 layers of three REBCO tapes wound on a stainless steel core. The primary parameters of these two cables are summarized in Table I and the details on the specification, design, and FLC performance of these cables can be found in [12].

In this article, coupled electromagnetic-thermal finite element modeling (FEM) simulations implemented in COMSOL Multiphysics [13] were developed and used to predict the FCL performance of the two tested cables with parameters shown in Table I. The simulated results were compared to the experimental data to validate and improve the simulation models. The FEM simulations were used to understand the electrical current redistribution due to temperature increase inside the cable during
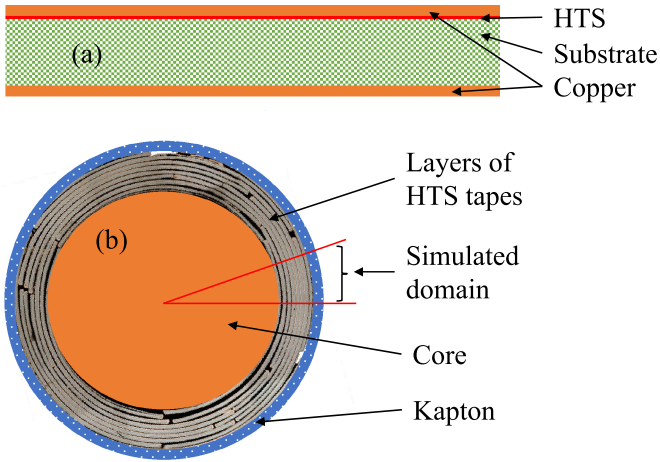
Fig. 1. (a) Cross section of a single REBCO HTS tape with all of its component layers. (b) Cross section of a typical REBCO CORC superconducting cable [14] consisting of a metal core inside and several layers of HTS tapes outside. Because of the symmetry, simulations can be performed in a small section.
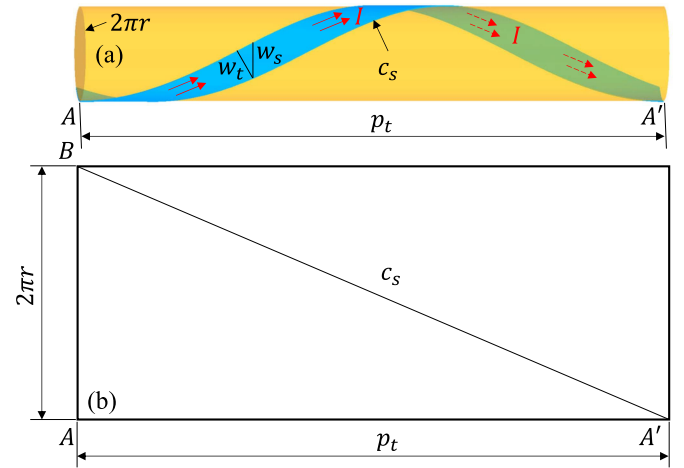

Fig. 2. (a) Illustration of the current running in a spiral path along an HTS tape. (b) 3-D cable surface is flattened into a 2-D plane to calculate the length of the spiral path c_s.

high-current pulses. These simulations can be used to optimize the cable design and estimate the heating that is needed for developing suitable cooling techniques.

II. FEM METHOD

An HTS REBCO tape structure usually consists of three electrically conductive components including the substrate, the superconducting layer, and the copper/silver stabilizer [see Fig. 1(a)]. Individual tapes are wound around a round core to form a CORC cable [14]. Fig. 1(b) shows the cross section of a typical CORC cable with a metal core, several layers of superconducting tapes, and a layer of insulation. During normal operation, the superconducting REBCO layers with approximately zero resistance will carry all the electrical current. When a fault happens, i.e., the transport current increases over the critical current of the cable, resistances of the superconducting layers will exponentially increase and the transport current will flow in the normal metal components, such as the tape substrate, its stabilizer, and the cable core. When electrical current starts flowing in the normal metal layers, heat will be generated inside the cable and temperature may increase significantly. Therefore, coupled electromagnetic-heat transfer FEM simulations are required to computationally model the performance of a superconducting cable during a fault.

A primary objective of this study is to understand current redistribution and temperature rise in individual layers over the cross section of the cable. With many tapes and several very thin layers in each tape, 2-D simulations were opted to perform in the cross section of the cable to reduce the computational burden. Because of the symmetry, simulations can be performed in a small section as shown in Fig. 1 to further reduce the computational load. Since the actual thicknesses of the HTS layers are about 1–3 μm and the meshing will be very heavy for these high-aspect-ratio layers if the actual thickness is used.

This challenge can be overcome with an acceptable computational error by artificially increasing the thickness of the HTS layers by several folds and simultaneously reducing the physical properties such as critical current density, thermal conductivity, and specific heat of those HTS layers by the same ratio. In our simulations, the thickness of the HTS layers is 5 μm, about three times the actual thickness of REBCO layers.

The spiral effect: In CORC cables, HTS tapes are wound in a helical fashion around a core. The current sharing between the winding layers strongly depends on contact resistance between the layers and how the HTS tapes in each layer are laid down around the core. This will be a complicated process and can only be simulated when information on the contact resistance and tape winding is provided. In this article, we investigate two extreme cases to compare with the experimental results. In the first case, HTS tapes are assumed to be fully insulated (or with very high contact resistance) and current sharing between the winding layers is negligible. In this case, transport currents will flow in the spiral winding path along the HTS tapes; therefore, the cross section and length of the current path are different from what is used in the 2-D simulations, which consider the current run straight along the cable. As seen in Fig. 2(a), the cross section of the current path within an HTS tape is presented by w_t, the width of the tape while the cross section in 2-D simulation is represented by w_s. Similarly, the current path in simulation is assumed to flow straight from point A to A′ with the length of the winding pitch p_t while in fact the current will flow in the spiral path along the HTS tape with the length $c_s = \sqrt{((2\pi r)^2 + p_t^2)}$ [see in Fig. 2(b)]. It is quite simple to accurately correct these geometry errors in the simulation by using the effective electrical conductivity of the metals, which is determined by multiplying the actual electrical conductivity with the correcting factor k given by

$$k = \frac{w_t}{w_s}\frac{p_t}{c_s} = \left(\frac{p_t}{c_s}\right)^2. \tag{1}$$
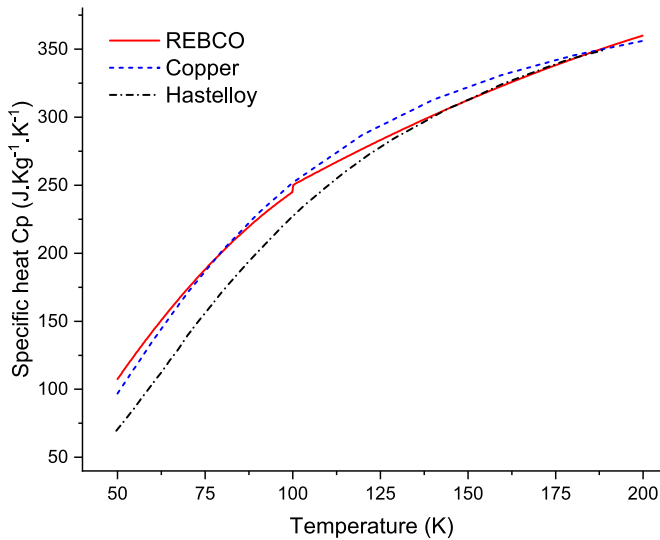
Fig. 3. Temperature dependence of the specific heat $C_p(T)$ of REBCO, copper, and Hastelloy.
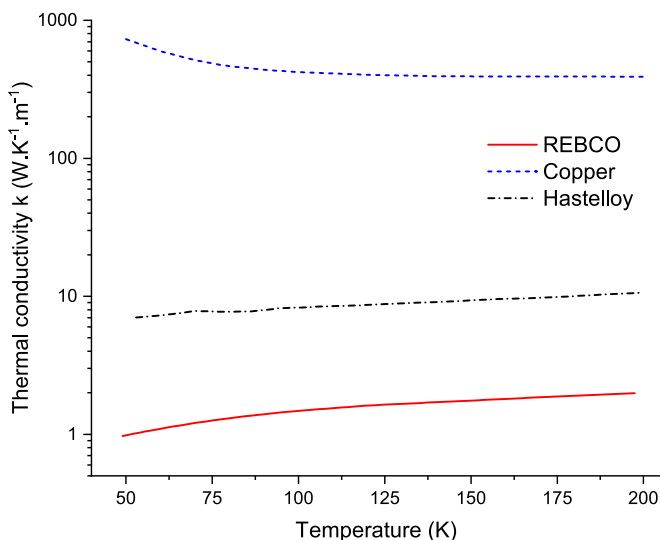

Fig. 4. Temperature dependence of the thermal conductivity $k(T)$ of REBCO, copper, and Hastelloy.

In the second case, the HTS tapes are assumed to be fully connected, i.e., the contact resistance between the winding layers is zero and the current during the fault condition ($I_{\text{cable}} > I_c$) will run straight along the cable by freely jumping from one winding layer to the next. The actual overcurrent performance of a cable is expected to be somewhere between these two extreme cases.

Material properties used in the simulations: To improve the computational accuracy, the temperature dependencies of electrical conductivity, specific heat, and thermal conductivity of all the materials must be considered in the simulations. The temperature dependence of electrical conductivity for copper and Hastelloy can be found in [15] and [16]. Figs. 3 and 4 plot the specific heat $C_p(T)$ and thermal conductivity $k(T)$ for all

REBCO, copper, and Hastelloy as a function of temperature between 50 and 200 K. The temperature dependence of thermal conductivity and specific heat of Kapton can be found in [17].

The superconducting property of REBCO layers is described by the standard power-law equation as follows:

$$E = E_0 \left(\frac{J}{J_c(T)} \right)^{n(T)} \qquad (2)$$

where $E_0 = 0.0001$ V/m, J_c is the critical current density of the superconducting layers, which is determined experimentally from the value of the cable critical current. If the critical current density J_c is determined from the critical current of individual HTS tapes, then the field dependence of critical current density $J_c(B)$ should be considered. In our case, J_c in winding layers were determined from I_c of the cable, so $J_c(B)$ is not necessary because the cable self-field is applied on the superconducting tape during the cable critical current measurement. The effective current density in each layer will be determined from the total critical current and the cross-sectional area of that layer. Since all the layers have the same number of tapes and the same thicknesses (i.e., the same layer I_c), the effective J_c of the outer layer will be slightly lower due to the slightly larger cross-sectional area. The temperature dependence of J_c must also be taken into account. This relation may vary slightly from tape to tape and in this article, we use [18]

$$J_c = J_0 \left[\left(\frac{T_0 - T}{T_0 - T_c} \right)^{1.5} + k_c \right] \qquad (3)$$

where $T_0 = 76$ K is the operating temperature of the cable and $T_c = 87$ K is the critical temperature, $k_c = 0.0001$ is a very small number added to avoid $J_c = 0$, which may cause a computational singularity. The value of $n(T)$ is not so important in the computational results, as long as it is high enough to create a sharp superconducting-to-normal transition. The n-value may fluctuate slightly with temperature and in our simulations, we assume that the n-value at 76 K is 23 and it is linearly decreased to 18 when the temperature reaches the critical temperature T_c.

III. RESULTS

A. CORC Cable With Copper Core (Cable 1)

The simulated and experimental electric fields in the CORC cable with the copper core as functions of time during a pulse are plotted in Fig. 5. In principle, when the driven current is lower than the cable I_c, the electric field is very small as expected. As seen in the figure, the computed result from the case of fully insulated tapes reproduces the experimental data very well while the simulated result with fully connected tapes is about 10% lower. With the high-conductivity copper core, electrical current flowing in the normal metal layers of the 2G HTS tapes during an overcurrent event is quite low, and therefore, the impact of the way these metal layers are treated either as fully insulated or fully connected on the computational results is insignificant. The very good agreement of the simulated results obtained with the case of fully insulated tapes to the experimental data indicates that the contact resistance between the tapes is high
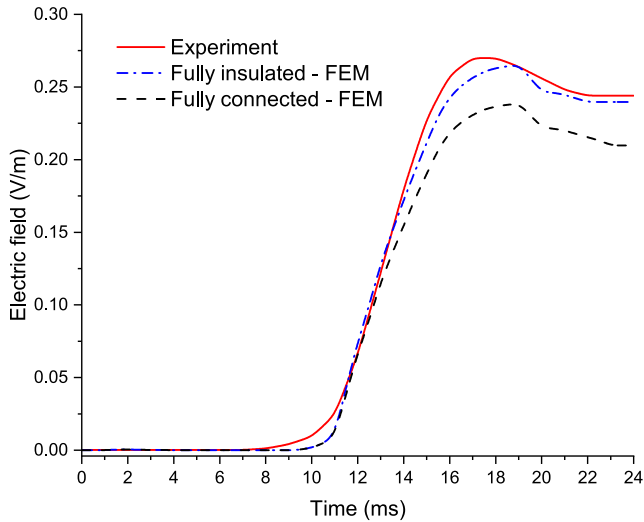
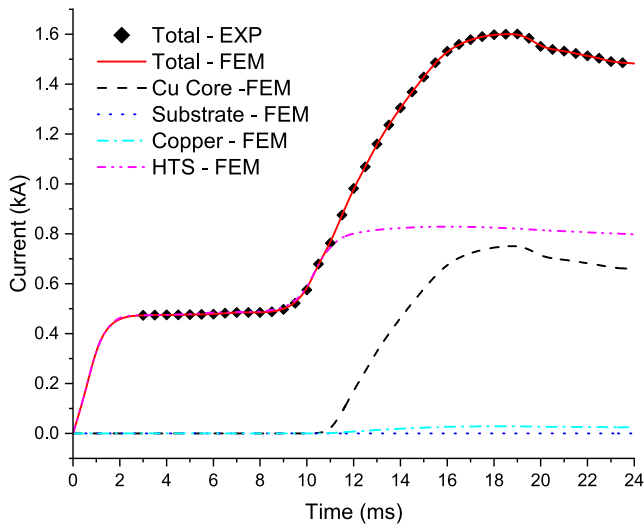Fig. 5. Experimental and simulated electric fields in the cable with copper core during an overcurrent pulse.

Fig. 7. Current density J_z (A/m^2) along the radial direction of the copper-cored cable at 5, 10, and 17 ms.

Fig. 6. Currents running in different cable components as functions of time for the copper-cored cable with the assumption of fully insulated tapes.

Fig. 8. Current density J_z (A/m^2) distributed in the cross section of the copper-cored cable at 5, 10, and 20 ms.

and the electrical current jumping between the winding layers through many surface contacts is low enough to be ignored in the simulations.

Fig. 6 plots the simulated aggregate electrical current pulses running in each layer component: the cable core, REBCO, substrate, etc., with time. The sum of these currents is the total current in the cable. As seen in the figure, the computed total current reproduces very well with the experimental data for the current pulse of 2.5 times $I_c(76$ K$)$, which is used as input for the simulation. When the current is lower than cable I_c, all the current is carried by HTS layers as expected. Current starts sharing to other components as total current increases above $I_c(76$ K$)$, around 11 ms. Because cable 1 was made with a large copper core, which has much lower electrical resistivity than that of the substrate layers in the 2G HTS tapes, a larger fraction
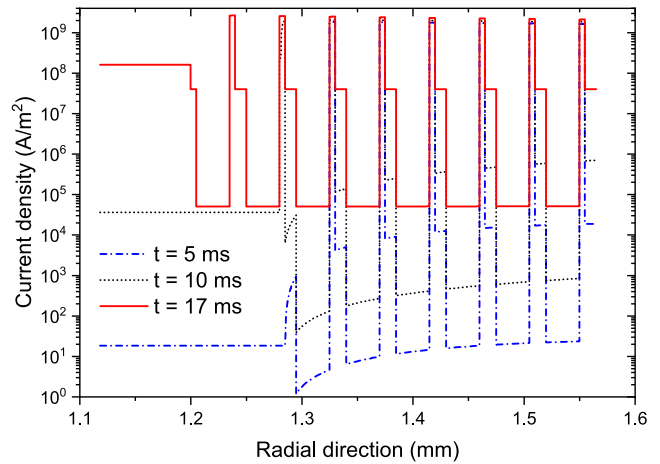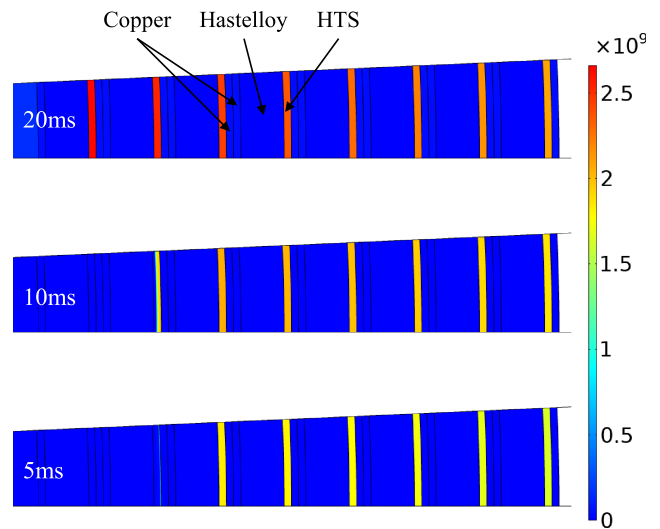
of the current is carried in the copper core. As seen in the figure, from 10 to 24 ms, the current in REBCO superconducting layers reaches about 0.8 kA while the current in the core increases from zero to 0.7 kA or 40% of the cable current. The currents in both core and REBCO layers gradually decrease from their peak values to slightly lower numbers at the end of the pulse. This reduction indicates that the cable temperature slightly increases during the pulse (more details on the distribution and evolution of cable temperature will be discussed later). The current in the substrate and copper layers of 2G HTS tapes is very low as expected. The current flowing in all the substrate layers is almost zero and the total current running in all the thin Cu layers is about 0.03 kA (or 2% of the cable current).

Figs. 7 and 8 plot current density distribution over the cross section of the cable at $t = 5$ ms, $t = 10$ ms, $t = 17$ ms, and $t = 20$ ms. At $t = 10$ ms, the current is reaching the cable I_c and only the REBCO layers carry the current. Because of the skin
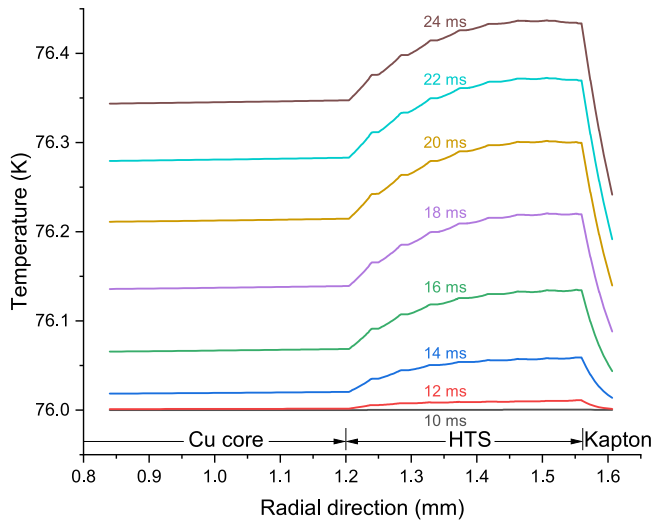
Fig. 9. Evolution of temperature along the radial direction with respect to time in the case of the copper-cored cable.

Fig. 10. Experimental and simulated electric fields in the cable with the stainless steel core during an overcurrent pulse.

effect, the outer REBCO layers were filled with electrical current first. The current in the innermost layer (layer 1) is basically still zero; layer 2 (the second innermost layer) is just partially filled with the current. The current density in the copper layers and substrate layers is also almost zero at this time. When the cable current is considerably higher than the cable I_c, such as at $t = 17$ ms, $(I_{\text{cable}} = 2.5I_c(76 \text{ K}))$, the HTS layers are saturated (see Fig. 8); the cable core and the normal metal layers of 2G HTS tapes start carrying a higher current but the current density is still much lower than that in the HTS layers. The current density in the HTS tapes is nonuniform because the nonuniform temperature rise over the cross section of the cable and because the effective J_c of the outer layer is lower as discussed earlier.

The temperature distribution and evolution in the cross section of the CORC cable with copper core with respect to the radial direction are depicted in Fig. 9. Overall, the temperature increase in the cable cross section is only about 0.44 K for the entire overcurrent pulse. The temperature does not increase until $t = 10.5$ ms, or $I_{\text{cable}} = 1.05I_c(76 \text{ K})$. The REBCO layers are well within a superconducting state at that temperature range and they still carry most of the current as seen in Fig. 6. Because of the skin effect, the current grows from the cable surface inward during the fault. Consequently, the temperature is higher near the cable surface. The much higher current density in the HTS and Cu layers will result in higher heat generated in those layers. Thus, the temperature in the HTS and Cu layers is higher than that in the substrate layers and the temperature distribution in the cable winding area is slightly nonuniform as shown in Fig. 9.

B. CORC Cable With Stainless Steel Core (Cable 2)

The simulated and experimental electrical fields as a function of time for CORC cable 2 with a stainless steel core are plotted in Fig. 10. The numerical results obtained for both cases (fully insulated and fully connected tapes) are also plotted. The results obtained with the assumption of fully insulated tapes reproduce the experimental data quite well but the electric field obtained with the assumption of fully connected tapes is much lower than
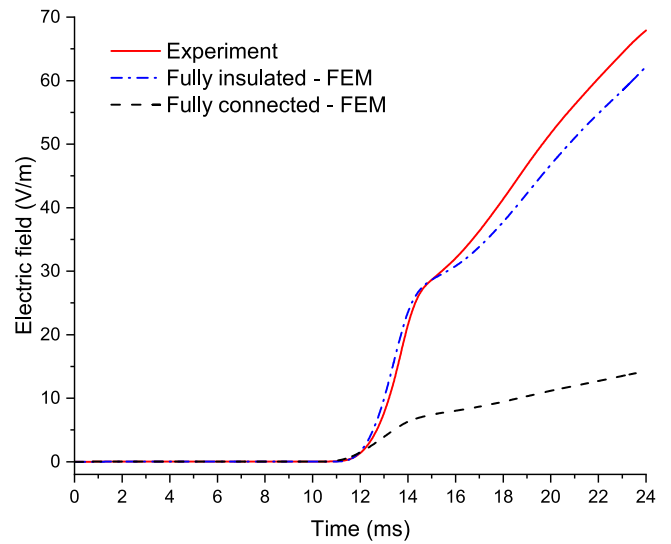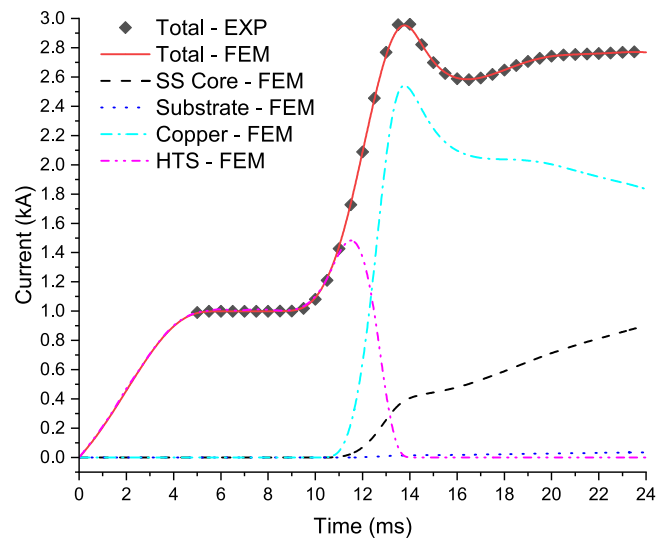

Fig. 11. Currents running in different cable components as functions of time for the stainless-steel-cored cable with the assumption of fully insulated tapes.

the experimental data. Unlike the copper-cored cable, the resistivity of the stainless-steel core is much higher, and therefore, the current that will be carried in the stabilizers and substrates of the HTS tapes will be much higher when the current is higher than the cable I_c. Consequently, the spiral effect of the cable winding is much stronger in the case of the cable with stainless steel core.

Fig. 11 plots the calculated electrical currents running in the HTS layers, the cable core, the Cu stabilizer, and the tape substrates as a function of time during an overcurrent pulse for the stainless-steel-cored cable, with the assumption of fully insulated tapes. The sum of these currents is the total current in the cable. As seen in the figure, the computed total current reproduces the experimental data very well of the current pulse that is used as input for the simulation. When the current is lower than cable I_c, all the current is carried by HTS layers as
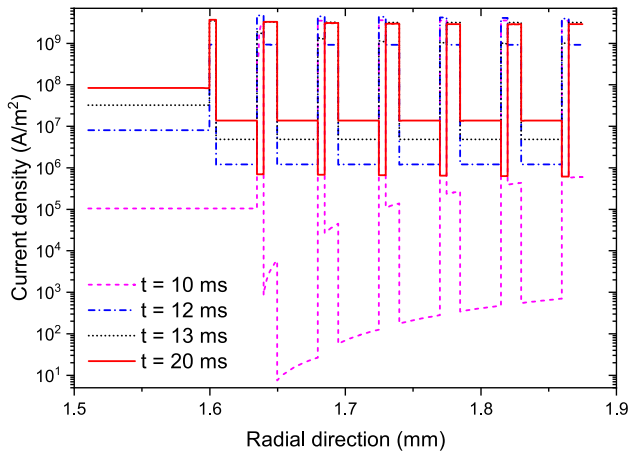
Fig. 12.   Current density J_z (A/m^2) along the radial direction of the stainless-steel-cored cable at 10, 12, 13, and 20 ms.

Fig. 13.   Current density J_z (A/m^2) distributed in the cross section of the stainless-steel-cored cable at 10, 12, 13, and 22 ms.

expected. Current starts sharing to other components as total current increases above I_c(76 K), around 11 ms. Because the stainless steel core has a high electrical resistivity, a much larger fraction of the current is carried in the Cu layers, even though those layers are only 5 μm thick. Consequently, the temperature in the REBCO HTS tapes increases quickly, resulting in a fast drop of the current density in the REBCO layers when the cable current increases above I_c(76 K). At 13.5 ms, the current density in the HTS layers drops to about zero indicating that the temperature in HTS tape winding area is above T_c. When the temperature increases, the electrical conductivity of the copper also increases at a much faster pace than the electrical conductivity of the stainless steel core; therefore, more electrical current will be diverted from the copper stabilizer to the cable core near the end of the pulse. The electrical current carried in the substrate layers is very small for the entire pulse.

The evolution of current redistribution during the pulse caused by a temperature rise can be confirmed in more detail in Figs. 12 and 13 that depict the distribution of the current density over the cross section of the cable at several moments during the pulse. The current first fills in the HTS layers from the cable surface. Clearly, the current density in the copper stabilizer layers increases significantly and the current density in the superconducting layers quickly reduces to zero when the cable current increases to above I_c.

Obviously, the temperature rise plays a significant role in distributing the electrical current in components of this cable. Fig. 14 helps to understand the evolution of the temperature over the cross section of the cable during the overcurrent pulse. The temperature in the HTS winding increases significantly up to 189 K at the end of the pulse $t = 24$ ms. The higher temperature increase quickly eliminates the superconducting property of the REBCO layers and the current density in those layers is reduced to near zero as seen earlier in Figs. 11 and 12.

IV. DISCUSSION

Simulation errors: It is expected that the simulations performed with the assumption of fully insulated tapes would overcalculate the electric field in those cables because the current
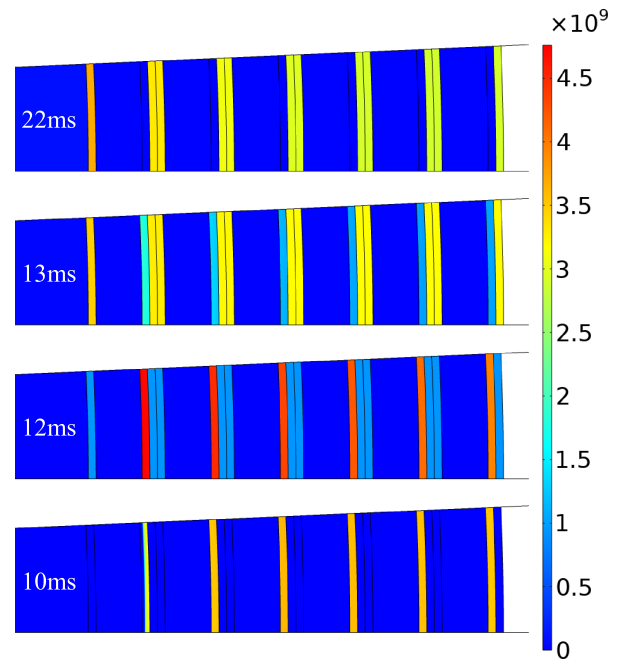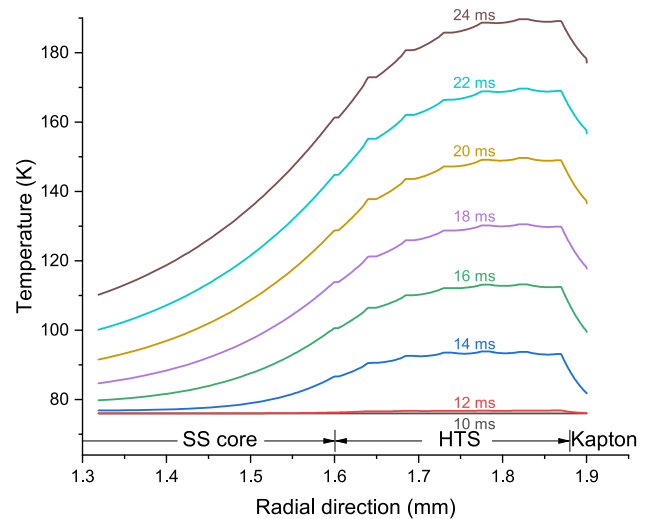
Fig. 14.   Evolution of temperature along the radial direction with respect to time in the case of the stainless-steel-cored cable.

sharing between winding layers was ignored in this assumption. In fact, the FEM results obtained with that assumption are slightly lower than the experimental data for both cables, implying that it is acceptable to assume that most of the transport current follows the spiral paths along the HTS tapes instead of transmitting through many contact surfaces for shorter paths. The high electrical resistance in contact between the layers may be a result of the fact that the HTS tape winding does not completely conform to the round surface of the cable while potential dog-boning in the copper layers will result in a relatively small contact surface area—between tapes [19].

Simulating the FCL performance for the cable with stainless steel core is much more challenging than for the cable with copper cores because, for a cable with copper core, most of the current exceeding the cable I_c will flow in the core, which is simpler to simulate. There would possibly be some additional causes for the computational errors that may need to be considered for improving the accuracy of the FEM simulations.

1) The temperature dependence critical $J_c(T)$ plays a very important role in the accuracy of the calculation, especially in the case of very fast and relatively high-temperature rise as seen in the cable with stainless steel core. However, the specification of $J_c(T)$ slightly varies from one type of REBCO tape to another and is very limited. Improving the accuracy of $J_c(T)$ will significantly improve the accuracy of simulations in general.

2) As seen in the simulation results, the copper layers carry most of the over-the-I_c current; thus, the thickness of the copper layers plays an important role in the accuracy of the simulations. It is challenging to control uniform thickness for a very thin (5 μm) copper layer along the wire and the relative variation of the thickness is higher for thinner Cu layers. This may be another important cause of the computational error, which is challenging to improve.

3) Finally, winding layers in the thermal simulations are treated as a continuous medium and the heat transfer resistance at the boundaries between the winding layers is ignored. However, HTS tapes in the real cables may not fully conform to the round surface, resulting in areas with reduced contact between layers. The thermal resistance at the boundaries should be evaluated and considered for better thermal transfer simulations. However, the thermal resistance at the boundary between layers will depend on the cable radius, HTS tape width, stiffness, and the tape winding tension. Thus, thermal resistance at the layer contact boundaries is not trivial to evaluate.

Simulation Challenges: One of the largest challenges for the simulations is handling the very high aspect ratio geometry of the thin layers in HTS tapes. To further reduce the meshing load for improving computational burden, several computational proximity approaches in the following can be used.

1) All, or several normal metal layers can be grouped into a single, equivalent metal layer with the effective conductivity, heat capacity, and the conductivity calculated from those physical properties of the constituent metal components and their volumetric fractions [20]. This proximity may introduce a computational error though. The electrical conductivity of copper is about 100 times higher than that of the Hastelloy substrates. Consequently, the current density and, therefore, heat generated in the copper layers will be much higher during the fault. Grouping metal layers into an equivalent layer will average out the heating in the normal metal layers. The simulated heat transfer to the HTS layers, in this case, may slightly differ from the fact that some copper stabilizers contact directly to the HTS layers and heat can be transferred very quickly to heat up the HTS layers and change their superconducting property.

2) To reduce the number of layers and increase the thickness of the HTS tapes, it is possible to group several superconducting layers into a single layer with effective thickness as the sum of the actual thicknesses of the grouped HTS layers. However, this treatment may also introduce some errors in both electromagnetic and thermal simulations. Because of the skin effect, the electrical current will penetrate from the cable surface toward its core as the current increases during a fault. The current density would be nonuniform and higher near the outer surface of the cable. This will result in a nonuniform temperature rise inside the cables. Grouping the superconducting layers into single, thicker layers will not truly describe the current sharing and temperature rise inside the cable, given the fact that the superconducting property of the HTS layers and the electrical conductivity of the normal metals strongly depends on the temperature.

V. CONCLUDING REMARKS

Comprehensive 2-D simulation models to predict the FCL performance of HTS CORC cables have been developed and validated against experimental data for two CORC cables, one with copper core and one with stainless steel core. The models with an assumption that HTS tapes are fully insulated and current only flows in the spiral path of the HTS winding reproduce the experimental data well and should be good enough to predict the FCL performance of the HTS cables. The models can calculate the current distribution in each individual component of the cable and individual layer of HTS tapes. The models can study the evolution of the current distribution and temperature over the cross section of the cable, thus enabling the assessment of the role of each component/layer in its FCL performance.

In the case of copper core, most of the current above the cable I_c will flow in the copper core and the temperature rise in the cable is minimal. For the cable with a stainless steel core, most of the current above cable I_c will be carried by the Cu stabilizers. In our case, the thickness of stabilizers is very thin, only 5 μm, and the temperature rise over the cross section of the cable is so significant that may eliminate the superconducting property of REBCO layers after several milliseconds of the fault. Thus, the thickness of the copper stabilizer plays the most important role in the FCL performance of the cable with stainless steel core.

REFERENCES

[1] H. Yumura et al., "Phase II of the Albany HTS cable project," *IEEE Trans. Appl. Supercond.*, vol. 19, no. 3, pp. 1698–1701, Jun. 2009.

[2] E. Y. Ko, S. R. Lee, S. Seo, and J. Cho, "Impact of smart HTS transmission cable to protection systems of the power grid in South Korea," *IEEE Trans. Appl. Supercond.*, vol. 29, no. 5, Aug. 2019, Art. no. 5402405.

[3] S. J. Lee, M. Park, I.-K. Yu, Y. Won, Y. Kwak, and C. Lee, "Recent status and progress on HTS cables for AC and DC power transmission in Korea," *IEEE Trans. Appl. Supercond.*, vol. 28, no. 4, Jun. 2018, Art. no. 5401205.

[4] M. Stemmle, F. Merschel, M. Noe, and A. Hobl, "Ampacity project– worldwide first superconducting cable and fault current limiter installation in a German City Center," in *Proc. IEEE 22nd Int. Conf. Exhib. Elect. Distrib.*, 2013, pp. 1–4.

[5] A. Ishiyama, X. Wang, H. Ueda, T. Uryu, M. Yagi, and N. Fujiwara, "Over-current characteristics of 275-kV class YBCO power cable," *IEEE Trans. Appl. Supercond.*, vol. 21, no. 3, pp. 1017–1020, Jun. 2011.

[6] M. Yazdani-Asrami, S. Seyyedbarzegar, A. Sadeghi, W. T. de Sousa, and D. Kottonau, "High temperature superconducting cables and their performance against short circuit faults: Current development, challenges, solutions, and future trends," *Supercond. Sci. Technol.*, vol. 35, no. 8, 2022, Art. no. 083002.

[7] D. Van Der Laan, J. Weiss, C. Kim, L. Graber, and S. Pamidi, "Development of CORC cables for helium gas cooled power transmission and fault current limiting applications," *Supercond. Sci. Technol.*, vol. 31, no. 8, 2018, Art. no. 085011.

[8] N. Riva, F. Sirois, C. Lacroix, W. De Sousa, B. Dutoit, and F. Grilli, "Resistivity of REBCO tapes in overcritical current regime: Impact on superconducting fault current limiter modeling," *Supercond. Sci. Technol.*, vol. 33, no. 11, 2020, Art. no. 114008.

[9] C.-H. Bonnard, F. Sirois, C. Lacroix, and G. Didier, "Multi-scale model of resistive-type superconducting fault current limiters based on 2G HTS coated conductors," *Supercond. Sci. Technol.*, vol. 30, no. 1, 2016, Art. no. 014005.

[10] S. Liang et al., "Study on quenching characteristics and resistance equivalent estimation method of second-generation high temperature superconducting tape under different overcurrent," *Materials*, vol. 12, no. 15, 2019, Art. no. 2374.

[11] H.-I. Du, T.-M. Kim, B.-S. Han, and G.-H. Hong, "Study on verification for the realizing possibility of the fault-current-limiting-type HTS cable using resistance relation with cable former and superconducting wire," *IEEE Trans. Appl. Supercond.*, vol. 25, no. 3, Jun. 2015, Art. no. 5402605.

[12] J. D. Weiss, C. Kim, S. Pamidi, and D. C. van der Laan, "Hybrid superconducting fault current limiting CORC wires with millisecond response time," *Supercond. Sci. Technol.*, vol. 32, no. 3, 2019, Art. no. 034005.

[13] [Online]. Available: www.comsol.com

[14] D. C. Van der Laan, J. D. Weiss, and D. McRae, "Status of CORC cables and wires for use in high-field magnets and power systems a decade after their introduction," *Supercond. Sci. Technol.*, vol. 32, no. 3, 2019, Art. no. 033001.

[15] J. Feng, "Thermohydraulic-quenching simulation for superconducting magnets made of YBCO HTS tape," Plasma Sci. Fusion Center, Massachusetts Inst. Technol., Cambridge, MA, USA, Tech. Rep. [Online]. Available: https://library.psfc.mit.edu/catalog/reports/2010/10rr/10rr007/10rr007_full.pdf

[16] J. Lu, E. Choi, and H. Zhou, "Physical properties of Hastelloy c-276^{TM} at cryogenic temperatures," *J. Appl. Phys.*, vol. 103, no. 6, 2008, Art. no. 064908.

[17] D. Rule, D. Smith, and L. Sparks, "Thermal conductivity of a polymide film between 4.2 and 300 K, with and without alumina particles as filler," *NISTIR 3948*, 1990. [Online]. Available: https://doi.org/10.6028/NIST.IR.3948

[18] F. Roy, B. Dutoit, F. Grilli, and F. Sirois, "Magneto-thermal modeling of second-generation HTS for resistive fault current limiter design purposes," *IEEE Trans. Appl. Supercond.*, vol. 18, no. 1, pp. 29–35, Mar. 2008.

[19] V. Phifer, M. Small, G. Bradford, J. Weiss, D. van der Laan, and L. Cooley, "Investigations in the tape-to-tape contact resistance and contact composition in superconducting CORC wires," *Supercond. Sci. Technol.*, vol. 35, no. 6, 2022, Art. no. 065003.

[20] E. Tsotsopoulou et al., "Modelling and fault current characterization of superconducting cable with high temperature superconducting windings and copper stabilizer layer," *Energies*, vol. 13, no. 24, 2020, Art. no. 6646.

Linh N. Nguyen received the B.S. degree in mechanical engineering from the Ho Chi Minh City University of Technology, Ho Chi Minh City, Vietnam, in 2010, the M.S. degree in computational engineering from Ruhr University Bochum, Bochum, Germany, and Vietnamese-German University, Ben Cat, Vietnam, in 2015, and the Ph.D. degree in mechanical engineering from Sejong University, Seoul, Republic of Korea, in 2020.

He is currently a Postdoc Research Associate with National High Magnetic Field Laboratory, Los Alamos National Laboratory, Los Alamos, NM, USA. His research interests include high-temperature superconductors, high-field magnets, finite-element modeling, and topology optimization.

Martin Naud is currently working toward the B.A. degree in mechanical engineering with the University of Waterloo, Waterloo, ON, Canada.

He has been with Los Alamos National Laboratory and the National High Magnetic Field Laboratory since 2019 developing high-performance mechanical systems for extreme environments and novel simulation models. While with LANL, NHMFL, and Waterloo, he has explored and focused on interdisciplinary problems. His research interests include complex systems, mathematical modeling, and fusion applications.

Jeremy Weiss (Member, IEEE) received the bachelor's degree in mechanical engineering and the Ph.D. degree in materials science and engineering from Florida State University, Tallahassee, FL, USA, in 2010 and 2025, respectively.

He is currently a Scientist with Advanced Conductor Technologies, LLC, Boulder, CO, USA, and a Research Associate with the University of Colorado, Boulder. At Florida State University, he studied as a member of the Applied Superconductivity Center from 2007 until 2015. He has an educational background that includes cryogenic and magnet design and has worked on the development of superconducting materials including YBCO, Bi-2212, MgB$_2$, and Pnictide wires. His present efforts include extensive improvements to the design and manufacture of CORC conductors to enhance performance while developing a more detailed understanding of the science behind high-temperature superconducting cables, wires, terminations, and joints for fusion and accelerator applications.

Sastry Pamidi (Senior Member, IEEE) received the Ph.D. degree in materials chemistry from the University of Bombay, Mumbai, India, in 1992.

He is currently a Professor with the Department of Electrical and Computer Engineering, FAMU-FSU College of Engineering, and is the Department Chair. He is also the Associate Director of the Center for Advanced Power Systems, where he also leads a multidisciplinary research group focusing on superconducting power applications. He collaborates with many research groups around the world and several small businesses. He delivered invited presentations at many international conferences. He authored and coauthored more than 200 publications in journals and conference proceedings and three book chapters. His research interests include high-power density superconducting devices, advanced characterization of superconducting devices and components, electrical insulation systems for cryogenic and superconducting applications, and applied cryogenics related to superconducting power applications, currently focusing on superconducting and cryogenic technologies for electric aircraft and ships.

Dr. Pamidi was a Guest Technical Editor for many special issues of IEEE TRANSACTIONS ON APPLIED SUPERCONDUCTIVITY. He is a Fellow of the Cryogenic Society of America.

Sven A. Dönges received the Diploma in physics from Christian-Albrechts-Universität zu Kiel, Kiel, Germany, in 2012, and the Ph.D. degree in physics from the University of Colorado, Boulder, CO, USA, in 2020.

He is currently a Scientist with Advanced Conductor Technologies, LLC, Boulder. His background is in ultrafast and cryogenic nano-optics with a focus on instrument design. He is currently working on design, development, and manufacturing of CORC conductors for power transmission, including cables, terminations, joints, and temperature interfaces.

Danko van der Laan received the Ph.D. degree in physics from the University of Twente, Enschede, The Netherlands, in 2004.

He is currently a Senior Research Associate with the University of Colorado, Boulder, CO, USA, and the Chief Executive Officer of Advanced Conductor Technologies, Boulder. He invented the Conductor on Round Core (CORC) cable, wound from high-temperature superconducting (HTS) REBCO tapes in 2009, and founded Advanced Conductor Technologies, LLC, Boulder, in 2011, to commercialize CORC cables. His research interests include the development of high-field magnets for particle accelerators and fusion reactors and HTS power cables for electric aircraft and naval applications.

Doan N. Nguyen received the B.S. degree in physics from Vietnam National University, Hanoi, Vietnam, in 2001, and the M.S. and Ph.D. degrees in physics from Florida State University, Tallahassee, FL, USA, in 2003 and 2007, respectively.

He has nearly 20 years of working in cross-disciplinary, spanning science and engineering of applied superconductivity, and high-field electromagnets. From 2007 to 2009, he was a Postdoctoral Associate with Superconductivity Technology Center (STC), Los Alamos National Laboratory, Los Alamos, NM, USA. From 2009 to 2012, he was a Technical Staff Member with STC. Since 2012, he has been offered to lead the pulsed magnet development program at Pulsed Field Facility, LANL, one of three campuses of the National High Magnetic Field Lab. In this role, he provides a broad array of analytical, computational, experimental guidance for the development, design, construction, and installation of ultra-high field pulsed magnets for users.